

Experimental methods in astroparticle physics

SS2020

Teresa Marrodán Undagoitia

Max-Planck-Institut für Kernphysik,
Saupfercheckweg 1, 69117 Heidelberg, Germany

E-mail: marrodan@mpi-hd.mpg.de

Contents

1	Lecture 7: Reactor neutrinos	2
1.1	Introduction	2
1.2	Reactors as sources of $\bar{\nu}_e$	3
1.3	Electron antineutrino detection	4
1.4	First neutrino detection: the Reines-Cowan experiments	5
1.5	Neutrino detection with organic liquid scintillators	6
1.6	Neutrino oscillation experiments	8
1.6.1	Neutrino oscillations	8
1.6.2	Ingredients in a reactor based oscillation experiment	9
1.6.3	Search for Δm_{12}^2	11
1.6.4	Search for Δm_{13}^2	13
1.7	Determination of neutrino mass hierarchy	15
1.8	Searching for sterile neutrinos	17
1.9	Coherent neutrino-nucleus scattering	20
1.10	Summary	20

1. Lecture 7: Reactor neutrinos

Neutrinos from nuclear reactors have played a crucial role in exploring neutrino properties, from the first direct observation of neutrinos in 1956 to the discovery of neutrino oscillation in 2001. This lecture is devoted to review reactor neutrino experiments, including neutrino production, the detectors that are typically used for detection, and the physics questions that can be answered. An interesting review about the topic of this lecture can be found in [1].

1.1. Introduction

The sources of neutrinos can be classified as natural, like neutrinos from the Sun, from astrophysical processes or from natural radioactivity, and artificial. Artificial sources include the neutrinos from accelerators which will be discussed in the next lecture but also reactor neutrinos. Figure 1 is an overview of neutrino sources in which their flux and spectral shape is shown. Reactors provide antineutrinos (in dark blue) with energies up to ~ 10 MeVs.

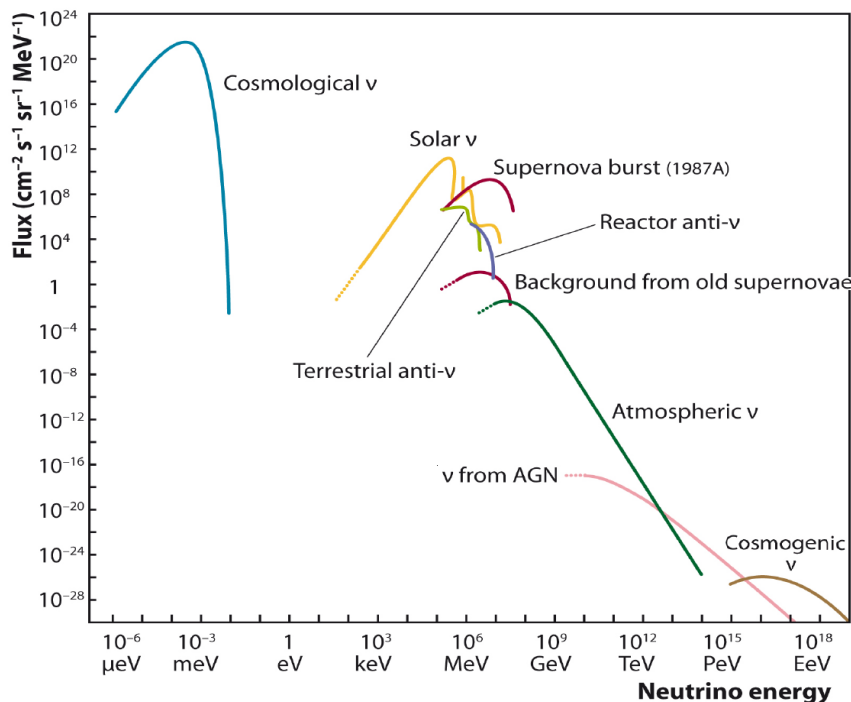


Figure 1. Spectral shape of various neutrino sources. Figure from [2].

Obviously, reactors emit $\bar{\nu}_e$ in a completely isotropic way. Together with the modest interaction cross-sections available at low energy, this makes signal rates rather low. At the same time, the low energy neutrinos provide us with a unique opportunity to probe the lowest regions of oscillation parameter space that are otherwise beyond the reach of accelerator-based searches.

1.2. Reactors as sources of $\bar{\nu}_e$

Reactors are a high intensity isotropic source of electron antineutrinos, $\bar{\nu}_e$. Each reactor core is an extended, cylindrical neutrino source of about 3 m diameter and 4 m height. An interesting feature is that commercial reactors have typically a shut down of ~ 1 month every (1 – 1.5) years for fuel replacement and maintenance. Plutonium breeding over each such cycle changes slightly the antineutrino flux and spectrum and, therefore, needs to be taken into account for scientific results.

The antineutrinos are produced in β^- decays of neutron rich fragments of uranium and plutonium. Consider for instance the fission of $^{235}_{92}\text{U}$



$^{94}_{40}\text{Zr}$ and $^{140}_{58}\text{Ce}$ are the stable nuclei with the most probable atomic numbers from the fission of $^{235}_{92}\text{U}$. While these nuclei have together 98 protons and 136 neutrons, the fission fragments (X_1 and X_2) have 92 protons and 142 neutrons. For this reason, in average 6 beta decays (neutron to proton) are necessary to reach stable matter. Consequently, 6 $\bar{\nu}_e$ are released per fission in average. Given that each fission releases approximately 200 MeV, for a 3 GW thermal reactor power, about 6×10^{20} antineutrinos per second are produced. Overall more than 99.9% of the antineutrinos produced at reactors result from ^{235}U , ^{238}U , ^{239}Pu and ^{241}Pu . The neutrino spectra from these components are derived from direct measurements of electron spectra of thin layers of these materials.

As power reactors are located mostly in the northern hemisphere, the neutrino flux is highest at these locations. Figure 2 (lower panel) illustrates the neutrino flux distribution. It can be observed that the highest fluxes are located in north America, Europe and Asia.

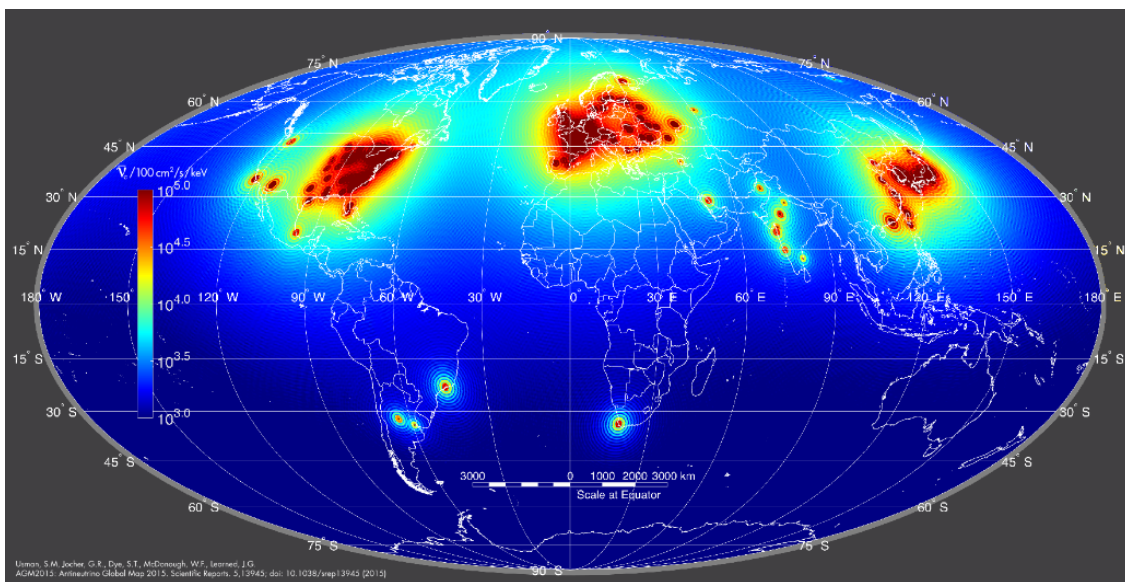


Figure 2. Reactor antineutrino flux worldwide. Figure from AGM2015: Antineutrino Global Map 2015, S.M. Usman et al., Sci. Rep. Vol. 5 (2015) 13945.

1.3. Electron antineutrino detection

The most common way to detect $\bar{\nu}_e$ is via the inverse beta decay (IBD) reaction



The energy threshold of this reaction is 1.804 MeV ($E_{thr} \sim m_n + m_{e^+} - m_p$) and therefore, only about 1.5 of the ~ 6 neutrinos produced in average per fission can be detected. Figure 3 shows the energy spectrum of $\bar{\nu}_e$, the IBD cross section as function of energy, and the observed energy spectrum for IBD events.

Exercise on this topic

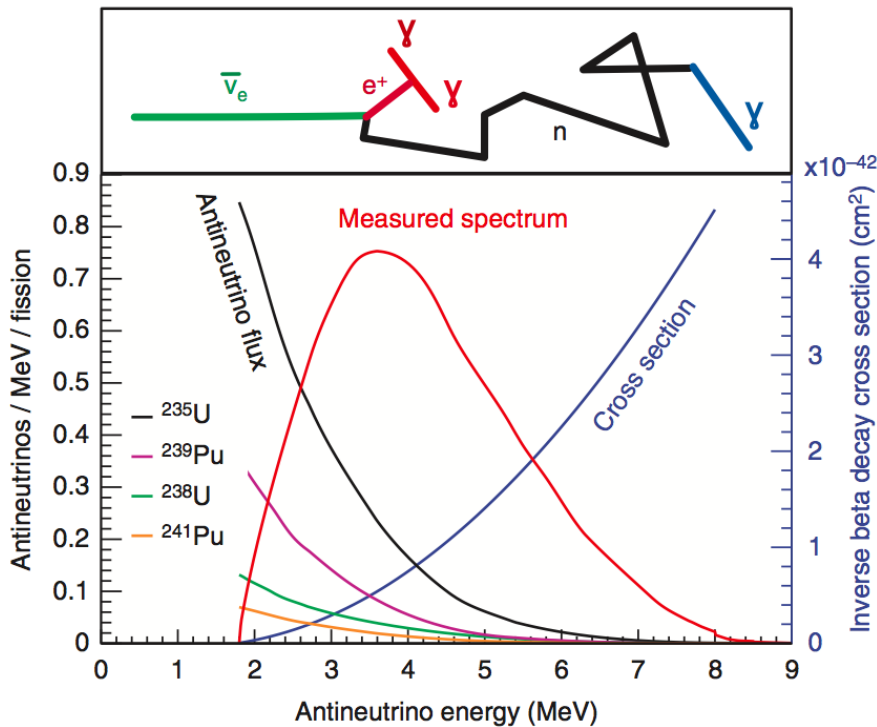


Figure 3. Energy spectrum of $\bar{\nu}_e$ from a reactor (black), the inverse beta decay cross section (blue) and the resulting observed spectrum (red). Figure from [3].

Experiments typically detect the coincidence between the prompt signal originating from the deposited energy by the positron and the delayed signal from neutron capture (see schematics on the top panel of figure 3). The neutron can be captured on hydrogen or on other element like cadmium or gadolinium for instance. For the neutron capture on hydrogen, the mean capture time is about 200 μs and results into the emission of a 2.2 MeV gamma:

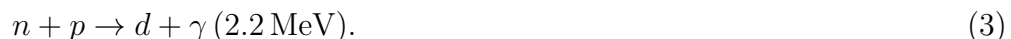


Figure 4 shows an image from an oscilloscope of a IBD event. After a small signal from the energy deposition by the positron, the gamma signal from the neutron caption can be seen. The figure is from the Savannah River experiment [4] which is described in section 1.4.

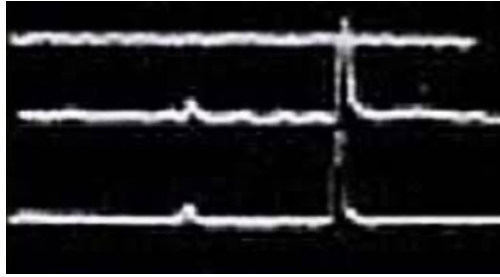


Figure 4. Scope picture with a typical IBD event signature. Figure from [4].

1.4. First neutrino detection: the Reines-Cowan experiments

The first neutrino detection was achieved by measuring antineutrinos from a nuclear reactor. It was reported by Reines and Cowan in 1953 [5]. They employed a 300 ton liquid scintillator detector loaded with cadmium for the target. The scintillation light produced was viewed by ninety 2-inch photomultipliers. A photograph of the experiment is shown in figure 5 (left).

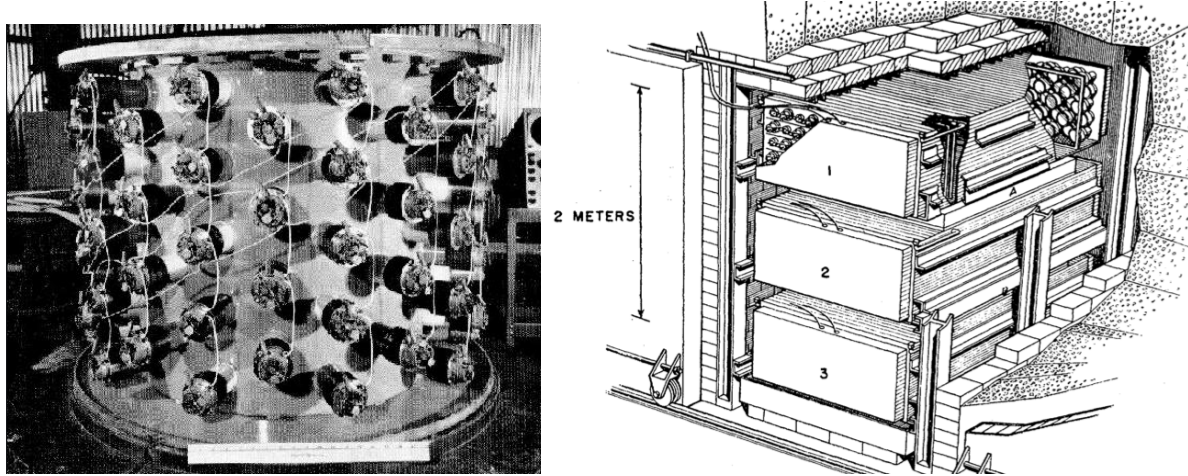


Figure 5. (Left) Photograph of the Reines and Cowan neutrino experiment. (Right) Illustration of the Savannah river experiment. Figure from [4].

Besides being relatively small, the detector look quite similar to current experiments at reactors. The $\bar{\nu}_e$ signal was detected via the inverse beta-decay reaction using the delayed coincidence between the positron and the gamma emission originating from the neutron caption on cadmium. Due to the high background, an inconclusive result was reported.

However, a few years later in 1956 Reines and Cowan performed an improved experiment [4] at Savannah River (Georgia, US). Two tanks were filled with 200 ℓ of water (A and B in figure 5, right). The protons in the water were the neutrino target and cadmium chloride dissolved in the water was used to capture the neutrons. The targets were in-between three large scintillator detectors (I, II and III) containing 1 400 ℓ

of liquid scintillator viewed by 110 PMTs each. The complete experiment was inside a lead shield. In April 1956, a clear signal had been observed. In contrast to the first experiment, the signal to background ratio was higher (3/1 compared to 20/1 before). Additionally, a first measurement of the neutrino cross section at $6.3 \times 10^{-44} \text{ cm}^2$ was reported with 5% error. At that time, the error on the predicted cross section was about 25%. This value had to be revised a few years later and resulted in a value approx. a factor of 2 above.

1.5. Neutrino detection with organic liquid scintillators

When a charged particle crosses a scintillating medium, it loses its energy mainly via electromagnetic interactions. Electrons of the medium instantaneously feel an intense electric field and molecules are either ionized or excited. In scintillating materials, part of the de-excitation energy is emitted in form of photons. The main advantages of such materials are: the linear relation between light output and energy deposition, the fast response time, and the possibility to apply pulse-shape particle separation.

Organic scintillators, as used in reactor experiments, consist of hydrocarbon molecules which contain benzene-ring structures. In order to form the hexagonal structure of benzene, a configuration in which carbon atoms share the so-called π -electrons is required. The resulting orbitals are symmetric with respect to the molecular plane (as shown in figure 6, left). A typical energy diagram for π -molecular orbitals is

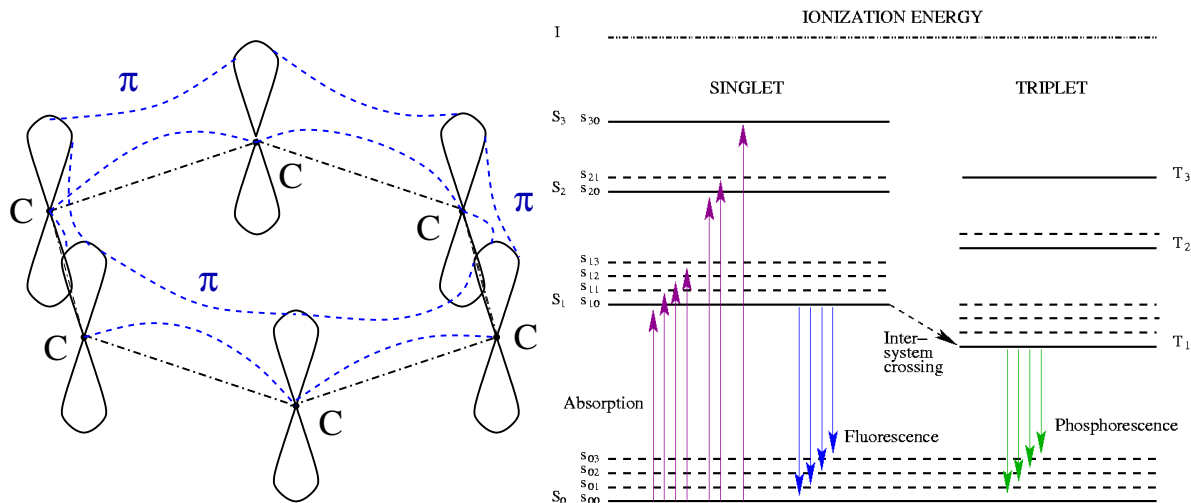


Figure 6. Left: orbital structure of the benzene rings showing explicitly π -orbitals. Right: π -orbitals in benzene: energy levels. Figures from [6].

shown in figure 6 (right). Depending on the relative spin orientation of the excited electron compared to the spin orientation of the unpaired electron in the ground state, parallel or anti-parallel relative spin orientations (singlet and triplet) can be defined. The spacings between electronic levels ($S_0, S_1 \dots$) are (2 – 4.5) eV while between the vibrational levels of the molecule ($S_{00}, S_{01}, S_{02} \dots$) is about 0.1 eV.

When some energy excites the molecule, it rapidly (10^{-12} s) dissipates its energy through collisions with neighbouring molecules until it reaches the S_1 level. As shown in the figure, fluorescence light is emitted through the transitions from S_1 to S_0 . Ionized molecules recombine with electrons mainly into excited states, 75% of them triplet states [7].

Once such triplet states are populated, there are several de-excitation paths. One possibility is the transition process T_1 to S_0 (phosphorescence), which is highly forbidden and therefore has a time scale of microseconds or longer. Usually the T_1 state produces indirect delayed-luminescence via $S_1 \rightarrow S_0$. Either the molecule acquires enough energy to return to S_1 , or collisions among T_1 can de-excite by the reaction:



where S^* is an excited singlet state. In both cases, fluorescence due to the S_1 to S_0 transition occurs but with a time delay compared to the direct emission. For energy depositions of particles with a high dE/dx , the probability for reactions as in equation 1.5 is higher and therefore, the amplitude of the triplet (slow) components is higher for protons or α -particles than for electrons, for instance. Figure 7 shows a diagram of the pulse shapes for different types of particles (normalized to the maximum of the emission). This allows organic scintillators to be able to separate between different

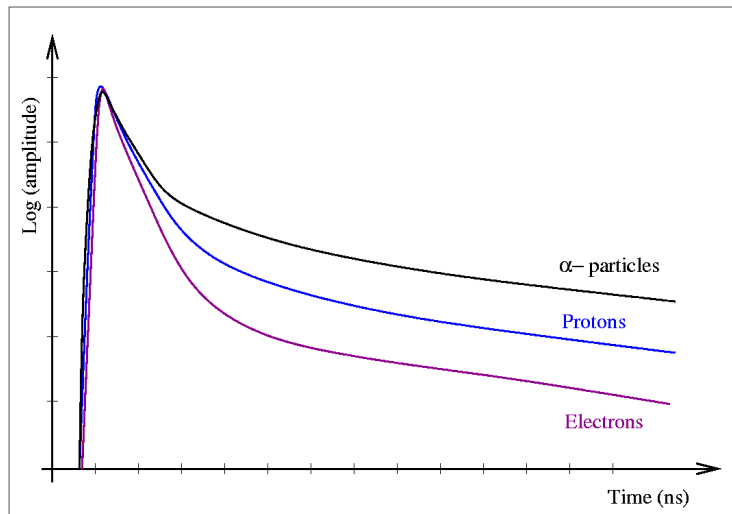


Figure 7. Schematics of the pulse shape for different types of particles in organic liquid scintillators. Figure from [6].

types of particles and can be used for signal identification or background rejection.

Organic scintillators are not transparent to their own scintillation light over large distances. For this reason, efficient wavelength-shifters are utilized. Low concentrations of wavelength-shifters are dissolved into the solvent providing a shift of typically ~ 50 nm.

In reactor neutrino experiments, the scintillator mixtures are loaded with a metal component in order to have a faster capture of the neutrons produced in the IDB reaction. An element with high de-excitation energy is convenient for a clear identification. Gadolinium is an example of a metal used for this purpose, it provides a shorter neutron capture time $\sim 20\mu\text{s}$ than hydrogen and it realises 8MeV in several gamma rays. The loading is a delicate process[8] as it should not affect the transparency of the medium and should stay stable (no fall-off) for the entire lifetime of the experiment which can be of several years. Finally, the scintillation light is recorded with photomultipliers.

1.6. Neutrino oscillation experiments

1.6.1. *Neutrino oscillations* As described in the previous lecture, oscillations between different neutrino flavour have been established having two distinct mass differences. These observations can be describe in an elegant way in a picture where the the neutrino flavour eigenstates (ν_e , ν_μ and ν_τ) are mixtures of the mass eigenstates (ν_1 , ν_2 and ν_3).

$$\begin{pmatrix} \nu_e \\ \nu_\mu \\ \nu_\tau \end{pmatrix} = \begin{pmatrix} U_{e1} & U_{e2} & U_{e3} \\ U_{\mu1} & U_{\mu2} & U_{\mu3} \\ U_{\tau1} & U_{\tau2} & U_{\tau3} \end{pmatrix} \begin{pmatrix} \nu_1 \\ \nu_2 \\ \nu_3 \end{pmatrix}$$

The mixing matrix is analogous to the mixing in the quark sector and it is often written in terms of three rotations and a CP violating phase δ_{CP} (only δ below).

$$\begin{pmatrix} \nu_e \\ \nu_\mu \\ \nu_\tau \end{pmatrix} = \begin{pmatrix} 1 & 0 & 0 \\ 0 & c_{23} & s_{23} \\ 0 & -s_{23} & c_{23} \end{pmatrix} \begin{pmatrix} c_{13} & 0 & s_{13}e^{-i\delta} \\ 0 & 1 & 0 \\ -s_{13}e^{i\delta} & 0 & c_{13} \end{pmatrix} \begin{pmatrix} c_{12} & s_{12} & 0 \\ -s_{12} & c_{12} & 0 \\ 0 & 0 & 1 \end{pmatrix} \begin{pmatrix} \nu_1 \\ \nu_2 \\ \nu_3 \end{pmatrix}$$

In the equation above c_{xy} and s_{xy} correspond to $\cos\theta_{xy}$ and $\sin\theta_{xy}$, respectively. θ_{xy} are the mixing angles between the mass states ν_x and ν_y where $x/y = 1, 2, 3$.

Antineutrinos from reactors have been successfully used to study neutrino oscillations. The mean energy of the detected neutrinos is between (3 – 4) MeV and therefore, only disappearance experiments are possible. In this experiments, a missing part of the flux (which oscillated to another flavour) is searched for. Muon or tau neutrinos cannot be produce due to the low energy of the neutrinos. In a two flavour scenario, the probability for a neutrino produced as electron neutrino to oscillate to a different flavour is given by:

$$P(\nu_e \rightarrow \nu_x) = \sin^2 2\theta \cdot \sin^2 \left(\frac{1.27 \cdot \Delta m^2(\text{eV}^2) \cdot L(\text{km})}{E_\nu(\text{GeV})} \right) \quad (5)$$

where Δm^2 is the mass splitting between the neutrino mass eigenstates, L the oscillation distance and E_ν the neutrino energy. *Exercise on this topic*

Reactor neutrinos can be employed to measure oscillation due to both Δm_{12}^2 (so-called 'solar mixing') and Δm_{23}^2 ('atmospheric mixing'). Using the mean energy of

reactor neutrinos, we can calculate the baseline for the oscillation maxima corresponding to the solar and atmospheric Δm^2 values:

$$\Delta m_{12}^2 \sim 8 \times 10^{-5} \text{ eV}^2 \rightarrow L \sim 70 \text{ km}, \quad (6)$$

$$\Delta m_{23}^2 \sim 2.5 \times 10^{-3} \text{ eV}^2 \rightarrow L \sim 2.5 \text{ km}. \quad (7)$$

Note that Δm_{12}^2 is two orders of magnitude smaller than Δm_{23}^2 .

Figure 8 shows the expected fraction of each neutrino flavour as function of distance for a neutrino energy of 4 MeV. Experiments search specifically for a deviation of the

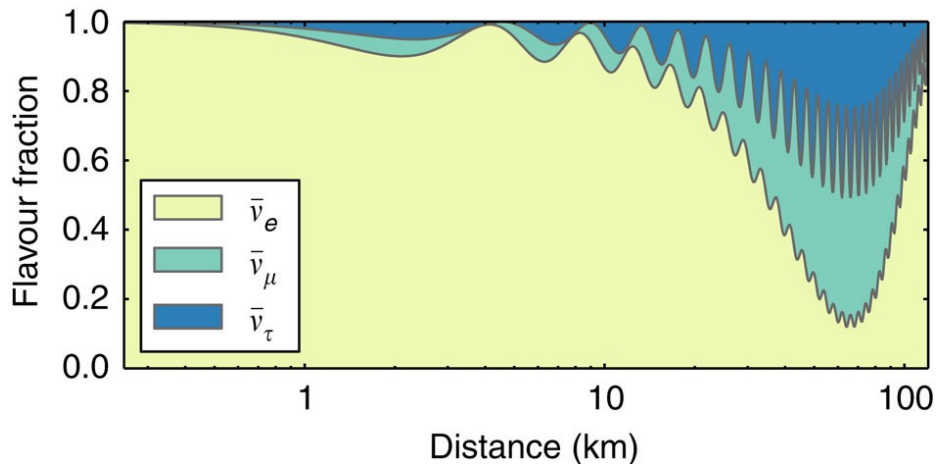


Figure 8. Expected flavour composition of the reactor neutrino flux, for neutrinos of 4 MeV energy used as an example, is plotted as a function of distance to the reactor cores. Figure from [3].

rate from the expected $1/r^2$ decrease due to the distance. Besides a simple counting of events, the observed spectrum (which is inferred from the positron energy) also contains information on the oscillations.

1.6.2. Ingredients in a reactor based oscillation experiment Several aspects are common for all reactor-based neutrino experiments and are briefly summarized below:

- Knowledge on the $\bar{\nu}_e$ flux and spectrum:

If only one detector is used, the flux needs to be calculated using the reactor thermal power and the reactor's fuel composition. As these quantities might not be known with great precision, experiments with two identical detectors are convenient. A near detector can be employed to measure the un-oscillated flux and spectrum directly.

- Detector acceptance:

For a given reactor neutrino flux, the acceptance gives the number of expected neutrino interactions. This calculation includes the distance from the reactor core, the size of the detector, the target mass, its composition and the efficiency of the selection criteria in the analysis.

- Background contributions:

As for other rare event searches, understanding and rejecting background is a key requirement in reactor neutrino experiments. Backgrounds are oft classified in two categories: uncorrelated and correlated.

The first type, uncorrelated, originate from random coincidences between two events. Together, they can by chance have the proper signature of an IBD event. An example of this background could be the coincidence between radioactive decay and a neutron produced by a cosmic muon. Luckily, uncorrelated backgrounds can be easily measured for instance by changing the time coincidence window.

Correlated backgrounds are in general more problematic and there are three main contributions: *Fast neutrons* are produced by cosmic rays and can mimic the IBD signature by scattering elastically off protons and subsequently being capture by Gd. In this case, proton recoils simulate the positron signal. An underground locations and shielding like vetoes (as for dark matter detectors) mitigate this component. However, if the muon is capture in insensitive material, its clear signal can not be identified. Spallation processes by cosmic rays muons can create *isotopes with a delayed signature* in the target. One example is ${}^9\text{Li}$ for which, in 50% of its beta decays, a neutron is produced. The coincidence of the beta electron and the neutron mimics the IBD neutrino signature. Similarly, an (α, n) -reaction on ${}^{13}\text{C}$ present in the scintillator can simulate the IBD signal. Figure 9 displays, as an example, the final result of a reactor neutrino experiment (KamLAND, see section 1.6.3). The bottom panel contains the

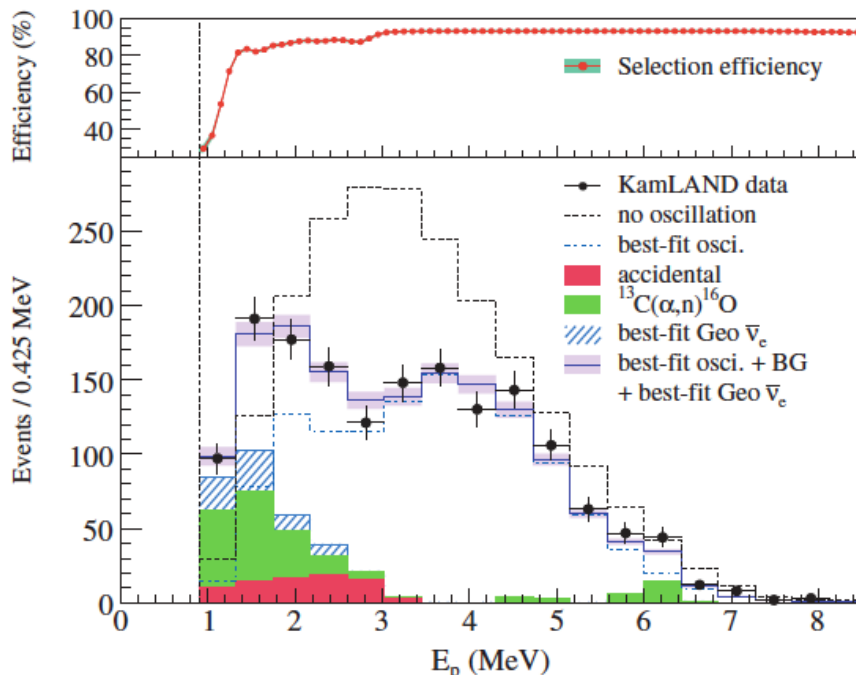


Figure 9. Detector efficiency and spectral results, Abe et al. (2008). Figure from [9].

expected non oscillated spectrum (dotted line), together with the data (black dots) and the best-fit oscillated spectrum (dashed blue). Three background components can be observed at low energies: random coincidences in red, the correlated background from (α, n) -reactions on ^{13}C in green and the geo-neutrino signal in dashed blue.

Finally, *geoneutrinos* are $\bar{\nu}_e$ created at β^- decays of ^{40}K , ^{232}Th and ^{238}U at the Earth crust and mantle. They have the exact same signature as the reactor neutrinos and are, therefore, an important background that has to be taken into account.

1.6.3. Search for Δm_{12}^2 Reactor experiments with baselines of about 70 km are sensitive to the solar mass splitting Δm_{12}^2 . The oscillation due to the mixing of ν_1 and ν_2 was first measured at solar neutrino experiments like SNO [10] and Superkamiokande [11].

Given the large baseline required to measure this oscillation, intense neutrino sources and large detectors are required. In addition, to clearly identify the signal over the background, a deep site is of interest. The Japanese experiment KamLAND was built to test solar neutrino oscillations. A diagram of the detector is shown in figure 10.

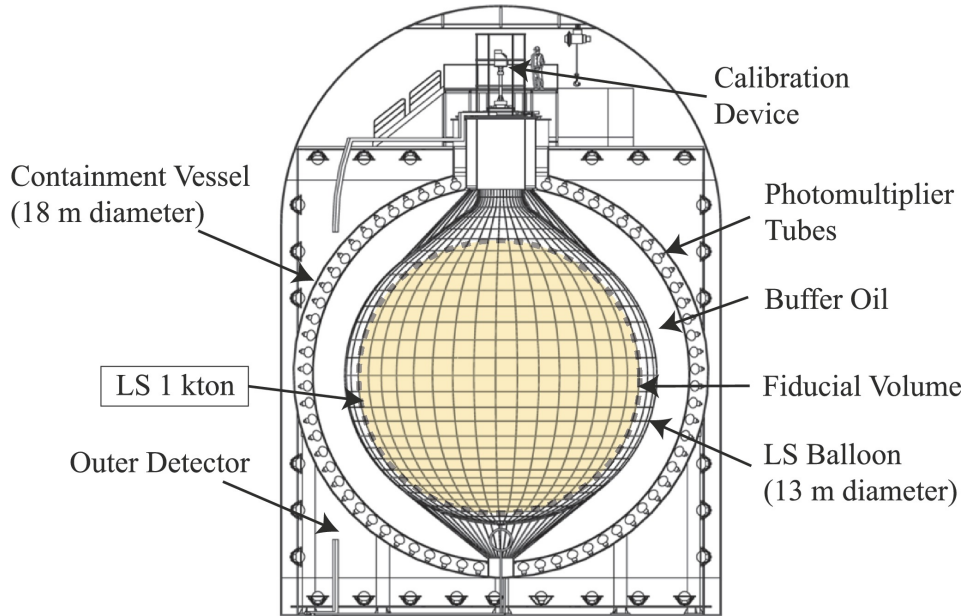


Figure 10. Schematics of the KamLAND experiment. Figure from Decowski et al. Nucl. Phys. B 908 (2016) 52.

The experiment is located at Kamioka under 2700 m.w.e. shielding and it's mostly sensitive to a limited number of baselines (note that many reactors are constructed in Japan). The target contains 1 kton of liquid scintillator inside a 13m ballon (in yellow). A 18 m diameter stain stell vessel holds the scintillator and has almost 1900 photomultipliers of 17 and 20 inch size. The region between the nylon ballon and the containment vessel is filled with mineral oil which acts as shielding for external radiation

(for instance gammas from the PMTs). Around the this vessel, there is a water-based Cherenkov detector to further shield the target and to record cosmic-ray muons.

The scintillator of KamLAND is not loaded with any metal and for this reason, the IBD signature utilizes the neutron capture on hydrogen (emitting 2.2 MeV) for the delay coincidence. Already in the first results of KamLAND in 2003, a clear deficit in number of events was observed:

$$\frac{N_{osb} - N_{bg}}{N_{exp}} = 0.611 \pm 0.085(stat) \pm 0.041(syst), \quad (8)$$

which is inconsistent with the $1/R^2$ flux dependence at 99.95% confidence level.

In a later publication in 2008, KamLAND performed a precise measurement of the parameters Δm_{12}^2 and θ_{12} [9]. The measured spectrum can be seen in figure 9 where a clear energy dependence of the oscillation probability can be observed. Figure 11 (left panel) shows the region of parameter space compatible with this event deficit at different confidence levels. The results are compared to the solar neutrino results.

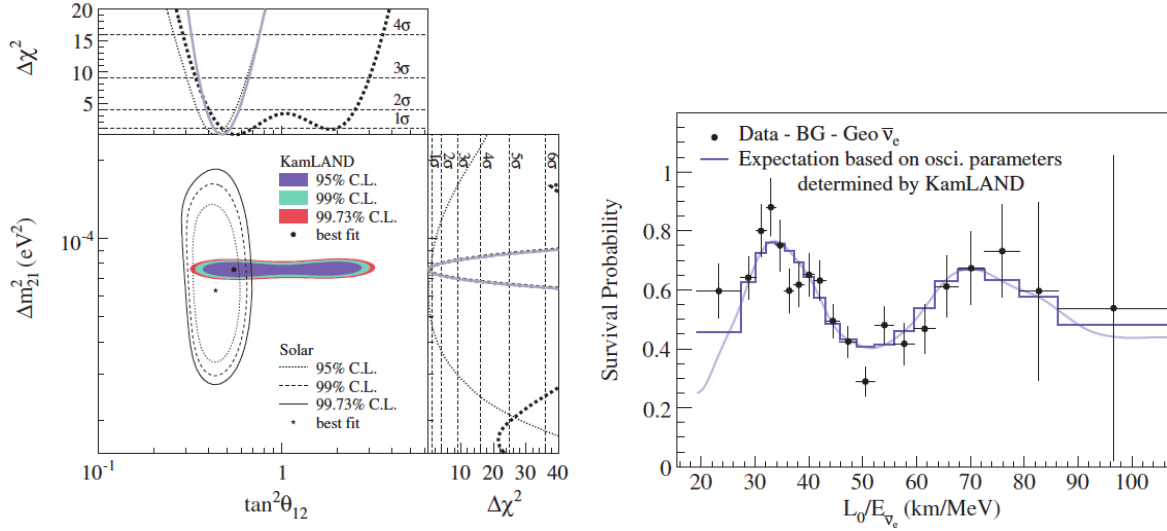


Figure 11. Left: allowed region for neutrino oscillation parameters from KamLAND and solar neutrino experiments. The side panels show the corresponding $\Delta\chi^2$ -profiles for KamLAND (dashed), solar- ν experiments (dotted) and the combination of both (solid). Right: Ratio of the background and geo-neutrino subtracted $\bar{\nu}_e$ spectrum to the no-oscillated expectation as a function of L_0/E . Figures from [9].

The right side of figure 11 shows the survival probability for $\bar{\nu}_e$ as function of L_0/E where $L_0 = 180$ km is the effective baseline taken as a flux-weighted average. The data points are determined subtracting the contribution from the background and geo-neutrino signals. The blue line is the expectation based on the oscillation parameters as measured by KamLAND.

Exercise on this topic

1.6.4. *Search for Δm_{13}^2* While the oscillations due to θ_{12} (solar) and θ_{23} (atmospheric) were measured by before 2005, oscillations due to θ_{13} were measured only about ten years later. In the Cabbibo-Kobasyashi-Maskawa (CKM) matrix for quark mixing, all three mixing angles are very small, however, in the neutrino mixing matrix they appear rather large. θ_{23} measured by atmospheric and long-baseline accelerator experiments is consistent with 45° and θ_{12} measured by solar searches and the KamLAND experiment is about 33° . It was therefore natural to expect the third mixing angle θ_{13} to be of similar size. θ_{13} is however, somewhat smaller.

The value of θ_{13} is important as it sets the scale to measure CP-violation. If θ_{13} would be equal to zero, there would be no possibility to measure CP-violation in neutrino oscillation experiments. The importance of knowing its value provoked a series of experiments world-wide including Double CHOOZ in France, RENO in Korea and Daya Bay in China. All these experiments have baselines around a kilometer and started data taking in 2011. They employed the same technology as some previous experiments in the 1990s, the gadolinium-loaded liquid scintillator. Gd has a high thermal neutron capture cross section. Only with $\sim 0.1\%$ gadolinium loading, the neutron capture time is reduced to about $28 \mu\text{s}$ from $\sim 200 \mu\text{s}$ for the un-loaded scintillator. The accidental coincident background is consequently, drastically reduced.

Typically two (or more) exact detectors are used, one of them being very close to the reactor/s (near detector) at a few hundred meters distance where no oscillations are expected, and another close to the expected oscillation maximum (far detector). Figure 12 shows as an example the layout of the Double CHOOZ experiment. The

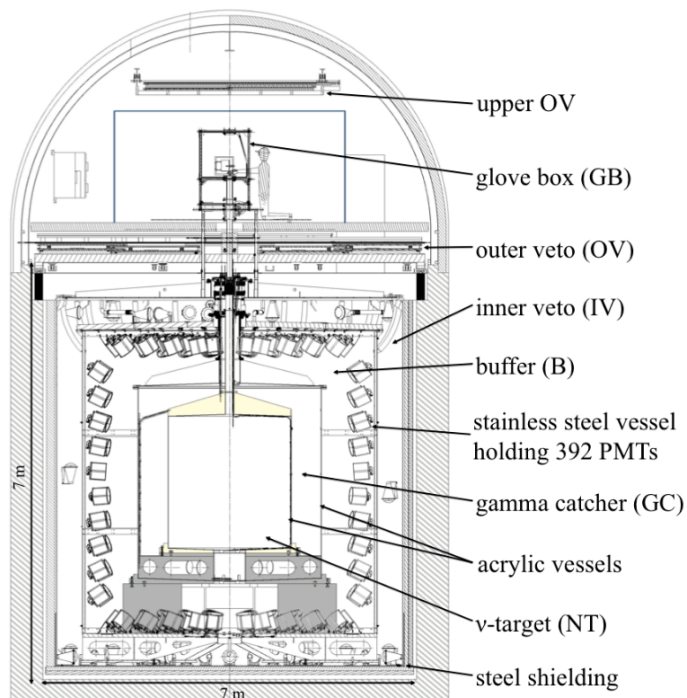


Figure 12. Schematics of the Double-CHOOZ detector system. Figure from [12].

experiments share an onion-like structure with several veto systems and a gamma catcher (not to miss the gamma emission from gadolinium) around the target.

The experiments were a great success. In 2012, all three Double CHOOZ [12], Daya Bay [13] and RENO [14] had reported clear evidence of neutrino disappearance at \sim a kilometer baselines after just a few month's running time. Figure 13 displays the first results of the Double CHOOZ experiment with a first indication of a flux deficit. The measured spectrum and the best-fit spectrum are shown together with the small

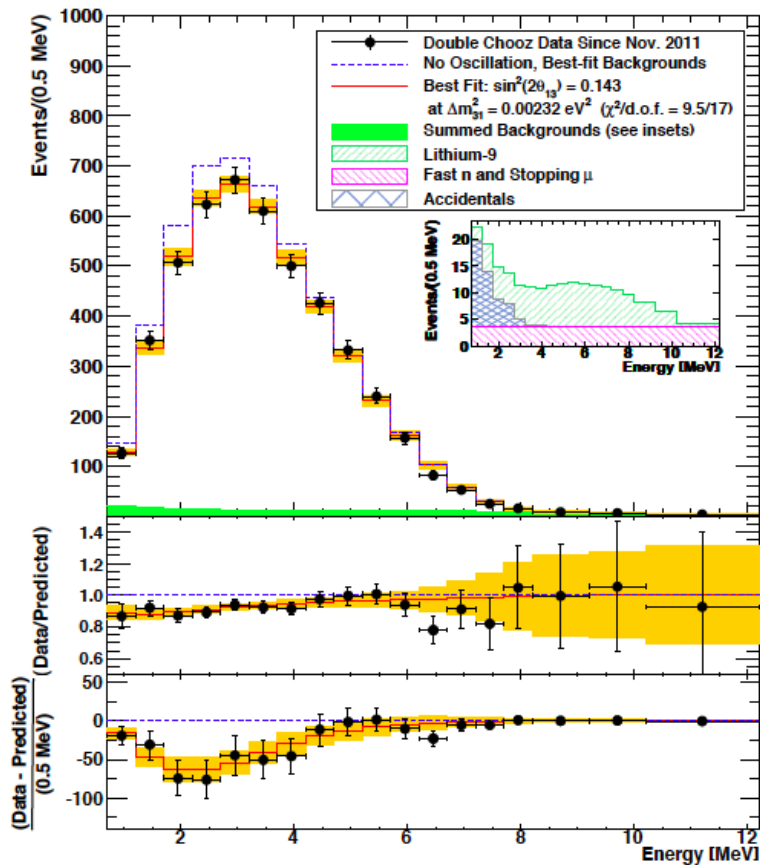


Figure 13. Results: antineutrino spectrum. Figures from Y. Abe et al. (2012). Figures from [15].

contribution of background from accidental and correlated backgrounds.

Among all experiments, Daya Bay had the largest reactor power (17.4 GW_{th} in total) and target mass (80 tons at the far site). Similar to the figure 11 (right) of KamLAND, the ratio of the detected $\bar{\nu}_e$ events to no-oscillation expectation at Daya Bay is plotted in figure 14. This experiment was built close to the six reactors of the Daya Bay nuclear power plant in southern China. Eight identical antineutrino detectors were used, two of them were placed at \sim 360 m from two of the reactor cores. Other two were placed at \sim 500 m and four at a far site at about 1580 m away from the reactor complex (see figure 14, right). This design allowed Daya Bay remove to a large extent

systematics due to correlated detector effects.

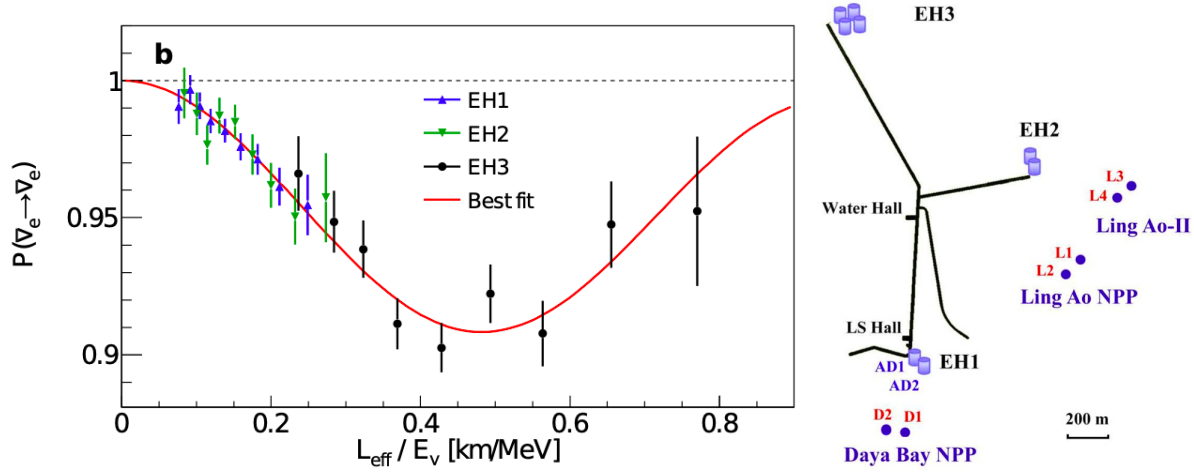


Figure 14. Left: Electron antineutrino survival probability versus propagation distance L over antineutrino energy E_ν . An effective detector-reactor distance L_{eff} is determined for each experimental hall (EH). Figure from [16]. Right: location of the six power reactors and eight detectors of the Daya Bay experiment. Figure from the experiment's homepage.

The combined data from the three experimental halls show an almost complete cycle of the expected periodic oscillation feature. The smaller amplitude and shorter wavelength of the oscillation, compared to the case of KamLAND, indicate the different oscillation component driven by the mass eigenstates ν_1 and ν_3 .

The best-fit of the oscillation of these experiments yields $\Delta m_{31}^2 \approx 2.4 \times 10^{-3} \text{ eV}^2$ and $\sin^2 2\theta_{13} \approx 0.1$ (also $\theta_{13} \approx 9^\circ$), which is consistent with the measurements at accelerator-based neutrino beams.

Exercise on this topic

1.7. Determination of neutrino mass hierarchy

From the oscillation experiments, only the absolute values of the neutrino mass-squared differences Δm_{31}^2 and Δm_{32}^2 are known but not their sign. From solar neutrino oscillations however, it is known that $\Delta m_{12}^2 > 0$ (related to matter effects in the Sun). The determination of the mass hierarchy is interesting because it would reduce the uncertainty in experiments aiming at the measurement of the CP-violating phase. In addition, it would help in defining the goals of the forthcoming neutrinoless double beta decay experiments and would improve our understanding of core-collapse supernovae [3].

Figure 15 shows a schematic of the two possibilities available for the ordering of the three neutrino masses:

- ν_3 heavier than ν_2 and ν_1 (normal hierarchy) or
- ν_3 lighter than ν_2 and ν_1 (inverted hierarchy).

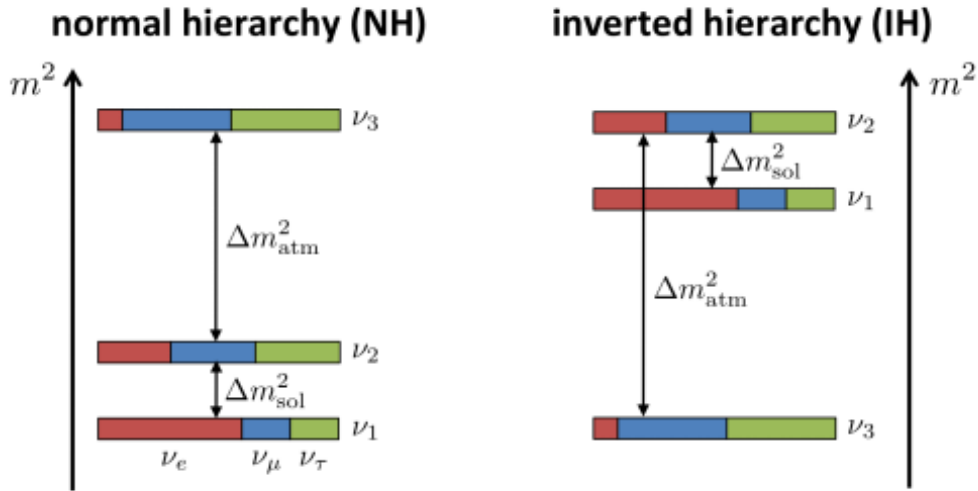


Figure 15. Schematics of the neutrino mass differences for normal (left) and inverted (right) hierarchy. Figure from M. Wurm.

Note that Δm_{sol}^2 is $\sim 10^{-5}$, the mass splitting Δm_{atm}^2 is of the order 10^{-3} .

As we have seen in the sections above, the reactor neutrino flux is modulated by the neutrino oscillations due to Δm_{12}^2 and Δm_{31}^2 . At an intermediate baseline, multiple small-sized oscillation peaks (due to $\sin^2 2\theta_{13}$) appear on top of the long oscillation due to $\sin^2 2\theta_{12}$. Depending on whether we have normal or inverted mass hierarchy, the small-sized oscillation pattern shifts slightly (see red and blue curves in figure 16). The mass hierarchy information can therefore be extracted from this pattern. Looking at

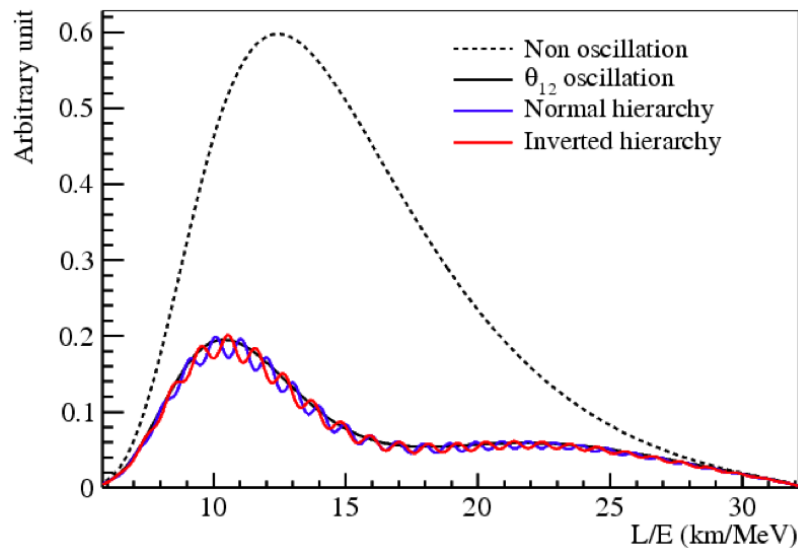


Figure 16. Relative shape difference of the reactor neutrino flux for normal and inverted hierarchy. Figure from [17].

figure 16 it becomes obvious that key aspects for a detector aiming to measure this shift are a superb energy resolution and an excellent energy calibration.

Exercise on this topic

JUNO [17] is an experiment under construction in southern China which aims to prove mass hierarchy with reactor neutrinos. The detector will be placed underground below 1800 m.w.e. and will measure neutrinos from two nuclear powers plans located at approx. 53 km distance. The difference between baselines to the two reactor complex is controlled to be within 500 m in order to prevent smearing of the mass hierarchy effect.

In order to collect enough statistics, massive detectors are required. Juno central detector consist of 20 kton liquid scintillator. The detector is quite similar to KamLAND (see figure 17), but is twenty times larger. To detect enough light from each event, the

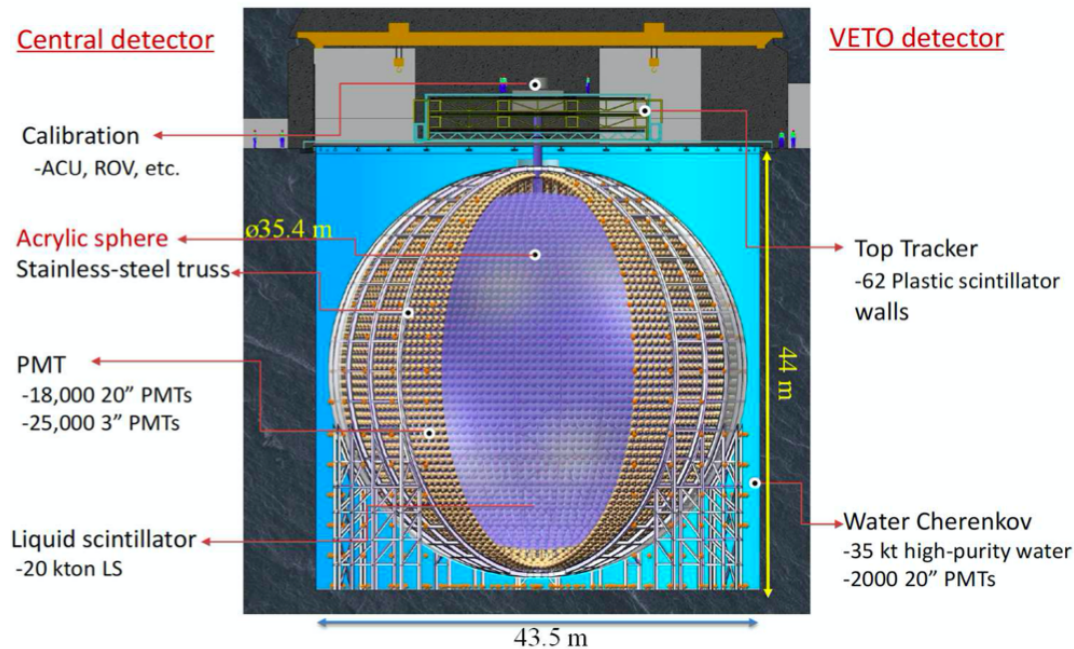


Figure 17. Schematic view of the JUNO detector including the central detector, the acrylic sphere, PMTs and veto systems. Figure from [18].

target is viewed by about 18000 photosensors of ≈ 50 cm diameter each. The high photon collection is essential to achieve the 3% energy resolution required to resolve the mass hierarchy-related wiggles. JUNO expects about 60 $\bar{\nu}_e$ events per day allowing to obtain a spectrum as displayed in figure 16. Its sensitivity is estimated to be above 3σ in 6 years measuring time.

1.8. Searching for sterile neutrinos

From precise measurements of the Z-boson decay width, the number of active neutrinos is determined to be 2.92 ± 0.05 [19]. Indeed, the three flavour scenario is very successful in describing the observations in solar, atmospheric, accelerator and reactor neutrino

oscillation experiments. However, there exist a few indications of additional neutrinos. As it doesn't interact with the Z-boson, it is called sterile neutrino.

One of the hints arises from the calibrations campaigns of the GALLEX [20] and SAGE [21] solar neutrino experiments with intense radioactive sources (^{51}Cr and ^{37}Ar). They observed a deficit in the expected ν_e rate, only 85% of the expected number of events were observed. This is known as 'gallium anomaly'. Interpreting this as due to oscillations to a sterile neutrino would point to a mass $\gtrsim 1\text{eV}^2$. Additionally, a new assessment of the reactor $\bar{\nu}_e$ flux resulted in an increased predicted rate for several experiments performed in the 90s (see experiments at small baseline (SBL) in figure 18). After correcting the outcome of these experiments with the new prediction, a 4 – 6%

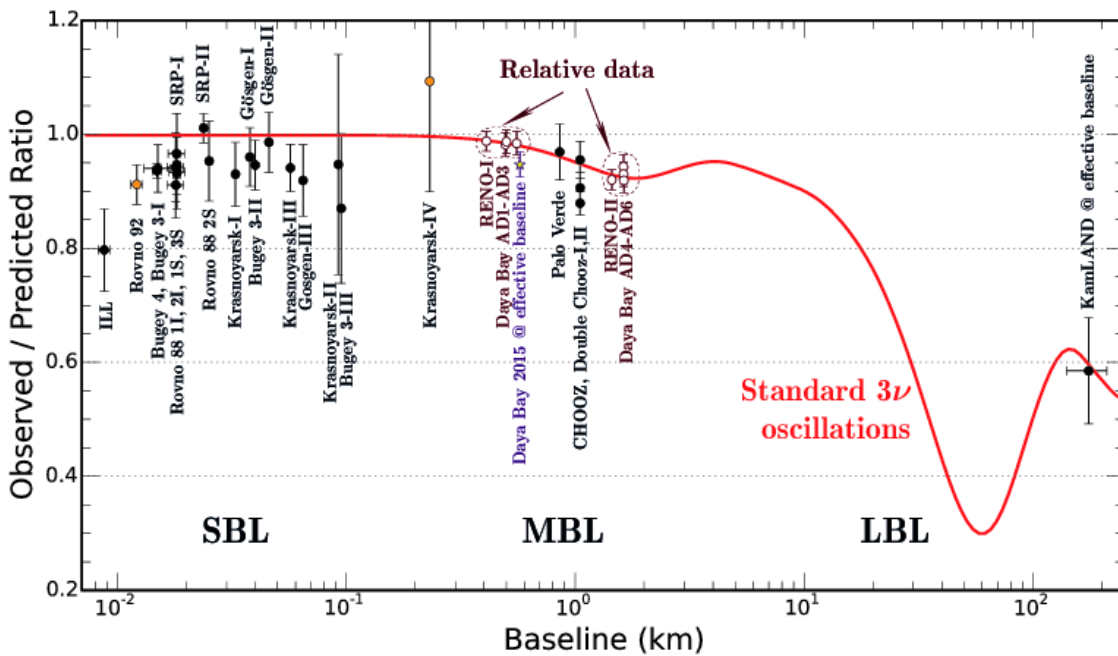


Figure 18. The reactor antineutrino anomaly. The data points represent the ratios between the measured event rates to the un-oscillated rates. Figure from D.V. Naumov, Phys. Part. Nucl. 48 (2017) 1, 12.

deficit resulted. This deficit is called 'reactor antineutrino anomaly' (RAA).

These experimental anomalies can be interpreted as being due to oscillation of neutrinos to light sterile neutrinos. If this would be the case, the preferred oscillation parameters would be around $\Delta m_{41}^2 \approx 1\text{eV}^2$ and $\sin^2 2\theta_{14} \approx 0.1$ (being ν_4 the sterile neutrino mass eigenstate). It has to be mention however, that the anomalies could be also explained by an imperfect knowledge on the theoretical predictions or due to experimental systematics. In order to test the sterile neutrino hypothesis, multiple short-baseline experiments of about 10m have been carried out worldwide. For this application, reactor cores of compact size are preferred to minimize the oscillations within the core. Those are research reactors, typically highly enriched in ^{235}U , in contrast to the commercial reactors in common nuclear power plants.

STEREO [22] is an example of such short-baseline experiments. The detector is installed at the high flux reactor of the Institut Laue-Langevin (ILL in France) whose compact core is 80 cm high and 40 cm diameter. It measures the $\bar{\nu}_e$ spectrum using a segmented target of six identical cells (37 cm length) which are filled with gadolinium loaded scintillator. The centers of each cell are placed at 9.4 to 11.1 m from the reactor core. Figure 19 displays a schematic representation of the detector.

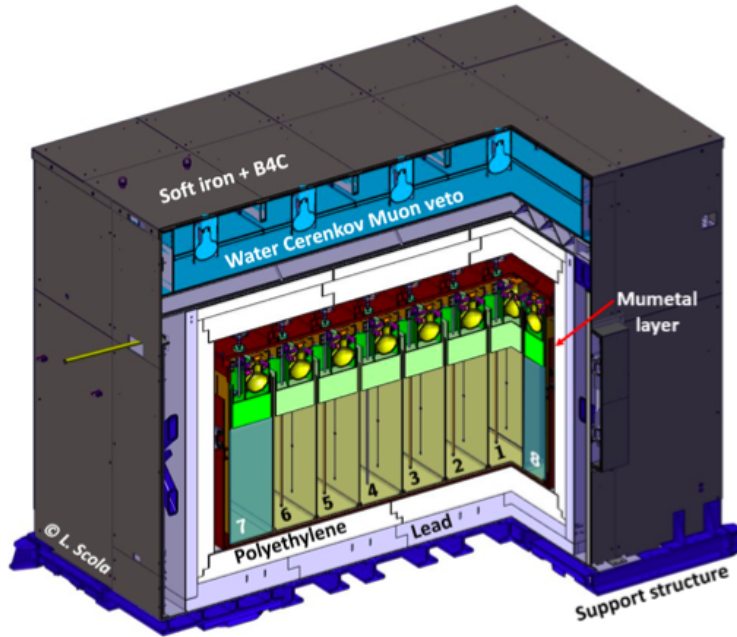


Figure 19. Schematics of the STEREO setup showing the target cells (1-6), the gamma catcher cells (7,8), muon veto and shielding. Figure from [22].

By comparing the measured $\bar{\nu}_e$ energy spectra of the different cells, the sterile neutrino hypothesis can be tested. Specifically, a neutrino oscillation with a mass splitting in the eV range would manifest in a spectral pattern of a distance-dependent distortion of the energy spectrum. STEREO data doesn't show a deviation from the non-oscillated expectation and therefore exclusion limits on the Δm_{41}^2 and $\sin^2 2\theta_{14}$ can be placed. Figure 20 gives an overview of experimental results. Note that this figure is from 2018 and, therefore, the results are eventually not the newest. The best fit of the reactor antineutrino anomaly (RAA) is shown (yellow star) together with the exclusion limits from NEOS (in Korea), DANSS (in Russia), STEREO and PROSPECT (in the US). The best fit RAA is excluded by the results of all these experiments at high significance. Also a large portion of the allowed region in this parameter space (unfortunately not shown in the figure) is excluded by this experiments. When taking into account these new experiments, the significance of the anomaly decreases.

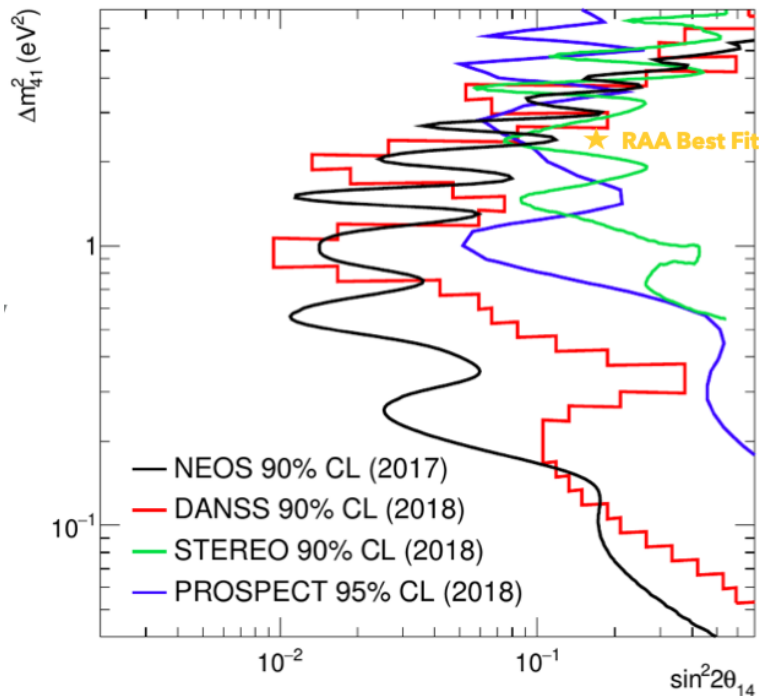


Figure 20. Sterile-neutrino search results from different short-baseline experiments. The best fit from RAA is also shown. Figure from a talk of Jaison Lee at PIC2018, Bogota, Columbia.

1.9. Coherent neutrino-nucleus scattering

Neutrinos from reactors can be employed to search for their coherent scattering off nuclei. So far this process has been measured only by using a neutrino beam from a stopped-pion neutrino source. The first measurement by the COHERENT experiment [23] employed a CsI target. Recently, the scattering on liquid argon has been also measured. There will be a dedicated lecture on coherent neutrino scattering experiments, therefore, no further details are given here.

1.10. Summary

In this lecture, reactors as sources of neutrinos have been discussed. The main detection reaction, the inverse beta decay, as well as the typical organic scintillator detectors were introduced together with the description of the first experiments of this type. We have reviewed the physics questions that can be investigated using reactor neutrinos including neutrino oscillations, neutrino mass hierarchy and the search for sterile neutrinos.

References

- [1] C. Bemporad, G. Gratta, and P. Vogel, “Reactor Based Neutrino Oscillation Experiments,” *Rev. Mod. Phys.* **74** (2002) 297, [arXiv:hep-ph/0107277](#).
- [2] C. Spiering, “Towards high-energy neutrino astronomy,” *Eur. Phys. J. H* **37** no. 3, (2012) 515.

-
- [3] P. Vogel, L. Wen, and C. Zhang, “Neutrino Oscillation Studies with Reactors,” *Nature Commun.* **6** (2015) 6935, [arXiv:1503.01059](#).
- [4] F. Reines, C. Cowan, F. Harrison, A. McGuire, and H. Kruse, “Detection of the free anti-neutrino,” *Phys. Rev.* **117** (1960) 159.
- [5] F. Reines and C. Cowan, “Detection of the free neutrino,” *Phys. Rev.* **92** (1953) 830.
- [6] T. Marrodán Undagoitia. PhD thesis, Technischer Universität München, 2007.
- [7] J. B. Birks, *The Theory and Practice of Scintillation Counting*. Pergamon Press, London, 1964.
- [8] C. Buck and M. Yeh, “Metal-loaded organic scintillators for neutrino physics,” *J. Phys. G* **43** no. 9, (2016) 093001, [arXiv:1608.04897](#).
- [9] **KamLAND** Collaboration, S. Abe *et al.*, “Precision Measurement of Neutrino Oscillation Parameters with KamLAND,” *Phys. Rev. Lett.* **100** (2008) 221803, [arXiv:0801.4589](#).
- [10] **SNO** Collaboration, Q. Ahmad *et al.*, “Direct evidence for neutrino flavor transformation from neutral current interactions in the Sudbury Neutrino Observatory,” *Phys. Rev. Lett.* **89** (2002) 011301, [arXiv:nucl-ex/0204008](#).
- [11] **Super-Kamiokande** Collaboration, S. Fukuda *et al.*, “Solar ^8B and hep neutrino measurements from 1258 days of Super-Kamiokande data,” *Phys. Rev. Lett.* **86** (2001) 5651, [arXiv:hep-ex/0103032](#).
- [12] **Double CHOOZ** Collaboration, Y. Abe *et al.*, “Indication of Reactor $\bar{\nu}_e$ Disappearance in the Double Chooz Experiment,” *Phys. Rev. Lett.* **108** (2012) 131801, [arXiv:1112.6353](#).
- [13] **Daya Bay** Collaboration, F. An *et al.*, “Observation of electron-antineutrino disappearance at Daya Bay,” *Phys. Rev. Lett.* **108** (2012) 171803, [arXiv:1203.1669](#).
- [14] **RENO** Collaboration, J. Ahn *et al.*, “Observation of Reactor Electron Antineutrino Disappearance in the RENO Experiment,” *Phys. Rev. Lett.* **108** (2012) 191802, [arXiv:1204.0626](#).
- [15] **Double CHOOZ** Collaboration, Y. Abe *et al.*, “Reactor electron antineutrino disappearance in the Double Chooz experiment,” *Phys. Rev. D* **86** (2012) 052008, [arXiv:1207.6632](#).
- [16] **Daya Bay** Collaboration, F. An *et al.*, “Spectral measurement of electron antineutrino oscillation amplitude and frequency at Daya Bay,” *Phys. Rev. Lett.* **112** (2014) 061801, [arXiv:1310.6732](#).
- [17] **JUNO** Collaboration, F. An *et al.*, “Neutrino Physics with JUNO,” *J. Phys. G* **43** no. 3, (2016) 030401, [arXiv:1507.05613](#).
- [18] A. Giaz, “Status and perspectives of the JUNO experiment,” in *Prospects in Neutrino Physics*, p. 53. 4, 2018. [arXiv:1804.03575](#).
- [19] **ALEPH, DELPHI, L3, OPAL, SLD, LEP EW Group, SLD Electroweak Group, SLD HF Group** Collaboration, S. Schael *et al.*, “Precision electroweak measurements on the Z resonance,” *Phys. Rept.* **427** (2006) 257, [arXiv:hep-ex/0509008](#).
- [20] F. Kaether, W. Hampel, G. Heusser, J. Kiko, and T. Kirsten, “Reanalysis of the GALLEX solar neutrino flux and source experiments,” *Phys. Lett. B* **685** (2010) 47, [arXiv:1001.2731](#).
- [21] **SAGE** Collaboration, J. Abdurashitov *et al.*, “Measurement of the solar neutrino capture rate with gallium metal. III: Results for the 2002–2007 data-taking period,” *Phys. Rev. C* **80** (2009) 015807, [arXiv:0901.2200](#).
- [22] **STEREO** Collaboration, H. Almazán *et al.*, “Sterile Neutrino Constraints from the STEREO Experiment with 66 Days of Reactor-On Data,” *Phys. Rev. Lett.* **121** no. 16, (2018) 161801, [arXiv:1806.02096](#).
- [23] **COHERENT** Collaboration, D. Akimov *et al.*, “Observation of Coherent Elastic Neutrino-Nucleus Scattering,” *Science* **357** no. 6356, (2017) 1123, [arXiv:1708.01294](#).